LA-UR-05-3393

Approved for public release; distribution is unlimited.

Title: Resolution Convergence and Sensitivity Studies with North Atlantic Circulation Models. Part I: The Western Boundary Current System

Author(s): Frank O. Bryan
Matthew W. Hecht
Richard D. Smith

Submitted to: Ocean Modelling

Resolution Convergence and Sensitivity Studies with North Atlantic Circulation Models. Part I: The Western Boundary Current System

Frank O. Bryan*
National Center for Atmospheric Research

Matthew W. Hecht, Richard D. Smith**
Los Alamos National Laboratory

*Corresponding Author: NCAR, POB 3000, Boulder, Colorado, 80303 USA
bryan@ucar.edu

**Present Address: POB 1342, Los Alamos, NM

Abstract

Numerical simulations of the general circulation of the North Atlantic Ocean in basin- to global-scale models have improved considerably in the last several years. This improvement appears to represent a regime shift in the dynamics of the simulated flow as the horizontal resolution decreases to around 10 km. Nevertheless, some significant biases in the simulated circulation and substantial uncertainties about the robustness of these results with respect to parameterization choices remain. A growing collection of simulations obtained with the POP primitive equation model allow us to investigate the convergence properties and sensitivity of high resolution numerical simulations of the North Atlantic, with particular attention given to Gulf Stream Separation and the subsequent path of the North Atlantic Current into the Northwest Corner. Increases in resolution and reductions in dissipation both contribute to the improvements in the circulation seen in recent studies. We find that our highest resolution eddy-resolving simulations retain an appreciable sensitivity to the closure scheme. Our most realistic simulations of the Gulf Stream are not obtained at the lowest levels of dissipation, while the simulation of the North Atlantic Current continues to improve as dissipation is reduced to near the numerical stability limit. In consequence, there is a limited range of parameter space where both aspects of the simulated circulation can be brought into agreement with observations. This experience gained with the comparatively affordable regional North Atlantic model is now being used to configure the next generation of ocean climate models.

1. Introduction

Simulations of the North Atlantic circulation with resolutions in the range of 1/9˚ to 1/12˚ conducted over the last several years [Paiva et al, 1999; Smith et al, 2000; Oschlies, 2002] have demonstrated considerable improvement in aspects of both the mean circulation and variability compared to earlier simulations with resolution in the range of 1/3˚ to 1/6˚ [Bryan et al, 1995; Beckmann et al, 1994; Chao et al, 1996; Willebrand et al, 2001]. This improvement appears to represent a regime shift in the dynamics of the flow as the horizontal grid size decreases to around 10 km. It has been argued that this is a result of the first baroclinic mode Rossby radius becoming resolved over most of the basin at this grid size, leading to adoption of the nomenclature "eddy-resolving" for the former and "eddy-permitting" for the latter. A prominent aspect of the improvement obtained in these cases is an apparent abatement of the Gulf Stream "separation problem" (Dengg et al, 1996). No less importantly, the path of the North Atlantic Current in the Northwest Corner region (Rossby, 1996) is also significantly improved. This area is often the site of the largest SST errors in both forced and coupled coarser resolution ocean general circulation models. Eddy-resolving ocean simulations have reached a stage where we can go beyond vague statements about "reasonable agreement" with observations to quantitative assessments of the verisimilitude of higher order statistical properties of the circulation [Bracco et al, 2002; McClean et al, 2002; Brachet et al, 2004].

Smith et al. (2000) (hereafter SMBH) compare their 0.1˚ North Atlantic model simulation results against those from a similarly, but not identically, configured 0.28˚ global model. Differences in forcing, different vertical resolution, and the regional versus global domains of the models made unambiguous attribution of differences in the solutions to horizontal resolution difficult. More recently, Oschlies (2002) has documented the improvements in aspects of the simulation of North Atlantic upon increasing the horizontal resolution from 1/3˚ to 1/9˚, where the vertical resolution, diapycnal mixing, topography and forcing are held fixed. In that study, the horizontal biharmonic viscosity and diffusivity were reduced by approximately one order of magnitude at the higher resolution, to the lowest values that prevented numerical instability. In terms of large scale features of the simulated general circulation, the changes obtained are broadly consistent with those of SMBH. Hurlburt and Hogan (2000) describe the changes in the simulation of the North Atlantic obtained with a hydrodynamic (no active thermodynamics) primitive equation model as the resolution is increased from 1/8˚ to 1/64˚. The results obtained at 1/8˚ share some of the features seen in the eddy-permitting simulations cited above, e.g., poor Gulf Stream separation and weak inertial recirculations, while those at 1/16˚ have some similarities to the 1/9˚ and 1/10˚ simulations of Oschlies(2002) and SMBH, e.g., improved Gulf Stream separation and more energetic recirculations. Hurlburt and Hogan show that the circulation, particularly the mesoscale variability, continues to change as the grid size is reduced further, with some suggestion of convergence at the highest resolution. Again, in this series of simulations the horizontal viscosity (harmonic in this case) is reduced in an apparently empirical fashion as the grid size is decreased.

In these and other studies, attribution of the improvements in the simulation to resolution alone has been hampered by other changes that have been made to the models concurrently, and by the complexity of the flow in the realistic domain and forcing settings of basin- to global-scale models. The values of eddy viscosity and diffusivity are generally adjusted to lower levels as the resolution is increased, typically to the lowest levels that prevent numerical instability of the model. Further, changes in the representation of topography, changes in forcing or sub-grid scale parameterizations between experiments, or even changes in the code between model generations present further complications that obscure the direct sensitivity of the solution to resolution of the flow, i.e., the true numerical convergence properties of the solutions.

In this study we investigate the sensitivity of the simulated circulation of the North Atlantic to changes in resolution between 0.4˚ and 0.1˚ using experiments in which the horizontal viscosity and diffusivity are adjusted along with resolution in the traditional manner, and in addition, in experiments where they are held fixed while the resolution is changed. Our primary objective in this study is to determine the degree to which the changes in the fidelity of the simulated flow are due to increased resolution versus decreased subgrid-scale dissipation. Additionally, we wish to determine the robustness of the highest resolution simulations, i.e., the degree to which they remain sensitive to sub-grid scale parameterization choices. In the present paper we establish the nature and magnitude of the model sensitivity; in subsequent studies analysis of the dynamical balances and budgets will be conducted.

The ability to broadly explore parameter space in the eddy-resolving regime has been greatly expanded by increases in computational speeds in recent years. As a comparison, the experiment described in SMBH required approximately 6 months to complete on a Thinking Machines CM-5, while more recent 0.1˚ experiments described here required only 1.5 weeks on an SGI Origin 3000 system.

In section 2, the model configuration and experimental design are described. In section 3 the results are presented. The changes in the circulation in the Gulf Stream region are described, first for the time mean vertically integrated transport, then for the transient (spin-up and short term variability) behavior of the Gulf Stream path. The sensitivity of the North Atlantic Current to changes in resolution and dissipation are described next, followed by a description of changes in the Deep Western Boundary Current system.

2. Model Configuration and Experiment Design

The North Atlantic model used in these experiments follows the configuration described in SMBH. The POP free surface, hydrostatic primitive equation code (Dukowicz and Smith, 1994) using z-coordinates, and a full-cell representation of topography is used. Mercator grids with zonal grid spacing of 0.4˚, 0.2˚, and 0.1˚ cover the Atlantic basin from 20˚S to 73˚N, including the Gulf of Mexico and the western Mediterranean. All cases use the same vertical grid with 40 vertical levels, varying in thickness from 10 m at the surface to 250 m in the deep ocean. The topography is interpolated to each grid

separately from the ETOPO5 digital terrain database, and key sills and passages have been hand edited to assure some consistency between grids and with bathymetric observations.

SMBH suggested that the horizontal biharmonic eddy viscosity, ν, and diffusivity, _, on the Mercator grid should be scaled with the cube of the local grid spacing. With this scaling the grid-scale Reynolds number

$$\mathrm{Re}_{grid} = \frac{U dx^3}{\upsilon} \tag{1}$$

is constant for a fixed velocity scale, irrespective of the location on the grid. In these experiments, we follow a similar prescription, but include an adjustable factor C in the expression for the eddy-viscosity:

$$\upsilon = C\upsilon_0 \left(\frac{dx}{dx_0} \right)^3 \tag{2}$$

where dx_0 =11.2km and $\upsilon_0 = -2.7x10^{10} m^4 s^{-1}$ are the equatorial grid spacing and reference viscosity on the 0.1˚ grid respectively, and dx is the local grid length. For the first series of experiments we follow the traditional procedure of reducing the eddy viscosity as the resolution is improved, using Equation 2 with C=1, to scale the viscosity across the different grids in the same way as it is scaled within each grid. In addition, we have carried out experiments with C varying between 0.125 and 8 on the 0.1˚ and 0.2˚ grids that allow us to separately examine the changes in the solution at fixed resolution with varying viscosity, and the changes in the solution with varying resolution at fixed viscosity. The biharmonic diffusivity is set proportional to the local biharmonic viscosity, with a Prandtl number of 3. The experiments described in this paper are summarized in Table 1, and the horizontal viscosity as a function of grid spacing for each case is shown in Figure 1.

All experiments are forced in the same way as described in SMBH using daily averaged wind stress computed from ECMWF TOGA surface analyses, the Newtonian cooling type thermal boundary condition of Barnier et al. (1995), and restoring of surface salinity to the Levitus (1982) monthly climatology. The north and south boundaries of the domain are closed to flow, and the temperature and salinity are restored to the annual mean Levitus climatology within 3˚ wide buffer zones.

An intermediate state of the experiment described in SMBH (referred to as experiment 13) provides the initial condition for experiments 13d and 13d2. In SMBH, a note added in proof indicated that fixing a bug in the code (the viscosity was erroneously scaled as dx^6 rather than dx^3), and modifications to the topography in the Lesser Antilles resulted in some improvements in the circulation in the Caribbean and Gulf of Mexico. The new run referred to there is experiment 13d in Table 1. The 0.2˚ experiment 15d follows a similar integration history as experiment 13d: it is started from an intermediate state of a

spin-up using a version of the code containing the viscosity bug. The lowest resolution experiment, 17d, is started from rest and follows the integration procedure described in SMBH: a five year spin-up period, followed by a 15 year production phase. Experiments 14a, 14b, and 14c are started from resting initial conditions and integrated for the period for which the wind stress forcing is available. The experimental configuration of experiments 13d and 14a are identical, they differ only in their initial condition. We present results from both as needed to allow one-to-one comparisons with other cases after the same length of integration or forcing period.

The spin-up of the circulation as measured by the basin mean kinetic energy is shown in Figure 2 for cases 14a, 14b and 14c. Due to the more complex spin-up procedures in the other experiments, we do not show their time series, but indicate the basin mean kinetic energy averaged over the last three years of each experiment . Similar to the results shown in Figure 2 of SMBH, the basin mean kinetic energy of the system approaches a stationary value on a timescale of approximately 10 years. For cases with viscosity on the C=1 curve (17d, 15d, 13d), the kinetic energy roughly doubles for each factor of two increase in resolution and corresponding factor of eight decrease in viscosity. For fixed viscosity the kinetic energy increases with increasing resolution, e.g., case 15d versus 13d2 or 15f versus 13d, more so at the lower level of viscosity. For resolution fixed at 0.1˚, the factor of 32 decrease in viscosity between cases 13d2 and 14c results in a doubling of kinetic energy.

3. Results

3.1 The Gulf Stream System

We first compare solutions at increasing resolution, in which the viscosity is scaled simultaneously with grid size according to Equation 2 with C=1. Beginning at the coarsest resolution, the 0.4˚ solution shown in Figure 3a, shows a transport pattern in the NW Atlantic familiar from many eddy-permitting models (Bryan et al, 1995; Dengg et al, 1996). The Gulf Stream separates from the boundary by first circulating around a strong anticyclonic "boundary eddy", then passes through a stationary wave pattern with amplitude decreasing in the downstream direction. There is no significant cyclonic recirculation to the north of the Gulf Stream, and the southern recirculation is weak and detached from the Gulf Stream itself. The path of the Gulf Stream is to the north of the observed mean path at all longitudes between Cape Hatteras and the Grand Banks. This separation structure is qualitatively consistent with that obtained in idealized barotropic (Cessi, 1991) and two-layer quasi-geostrophic models (Özgökmen et al, 1996) where it has been designated separation by "vorticity crisis".

At 0.2˚ (Figure 3b), the circulation pattern is qualitatively similar, with some quantitative differences. The boundary eddy centered at 36.5˚N, 71˚W strengthens from 50 Sv to 70 Sv, and the path of the Gulf Stream is south of that in experiment 17d, particularly east of 65˚W. From that longitude to the Grand Banks, the beginning of a cyclonic recirculation

is apparent to the north of the Gulf Stream. The southern recirculation weakens slightly compared to the 0.4˚ case.

At 0.1˚ (Figure 3c), the boundary eddy disappears, and the GS separates from the coast as a jet at Cape Hatteras. The northern recirculation cell extends all the way west to the separation point, and a vigorous southern recirculation has developed. The southern recirculation extends southwest along the boundary, resulting in enhanced Gulf Stream transport over the 0.2˚ experiment as far south as the Bahamas. Within the broad northern and southern recirculation gyres, there are a number of localized recirculating cells, with the anticyclonic cells in the southern gyre being stronger. There is a distinct break in both recirculation gyres near 59˚W coincident with the New England Seamount Chain, and another in the southern gyre at 70˚.

In the 0.2˚ experiment 15f (Figure 3d), the viscosity is reduced to the level used in the standard 0.1˚ experiment (13d or 14a). Comparing to the standard 0.2˚ experiment (Figure 3b) the factor of 8 reduction in viscosity results in a slight strengthening of the northern recirculation gyre (NRG) east of the New England Seamount Chain, but minor changes to the west near the separation point. The southern recirculation also strengthens, both to the west and the east of the NESC. The boundary eddy weakens somewhat from experiment 15d, but does not disappear as in experiment 13d (the 0.1˚ experiment with the same viscosity as experiment 15f). At this level of viscosity there are indications of increased grid-scale noise, possibly due to insufficient resolution of the Munk layer, or simply due to insufficient suppression of numerically-generated noise.

Another comparison of experiments at fixed viscosity with increasing resolution is provided by experiment 13d2 (Figure 3e) versus experiment 15d (Figure 3b). The recirculations north and south of the GS are slightly stronger in experiment 13d2 than in experiment 15d, and comparable to those in experiment 15f. The boundary eddy remains, but is shifted to the south and has slightly reduced amplitude compared to experiment 15d.

The differences between experiments 15f and 13d and between 13d2 and 15d, where the parameters are held fixed and the resolution is changed, are direct indications that the solution has not converged in the traditional numerical analysis sense. One might argue that the solution appears to be nearer to convergence for higher (undesirably so) values of viscosity.

Extending the parameter range of the 0.1˚ experiments to lower viscosities in experiments 14a, 14b, and 14c (Figure 4) shows further changes in the flow fields. With decreasing viscosity, the Gulf Stream separates from the boundary at a position south of the observed separation point at Cape Hatteras, and the recirculation gyres continue to strengthen. The spatial extent of the NRG expands (negative streamfunction values occupying a greater fraction of the area north of the GS). As was the case in the higher viscosity limit, the southern recirculation and its embedded cells strengthen more strongly than the northern recirculation.

The downstream transport of the Gulf Stream, computed in stream coordinates (using the methodology described in SMBH) for the 0.1˚ experiments is shown in Figure 5. As is apparent from the streamfunction in Figures 3 and 4, the barotropic component of the transport increases substantially with decreasing viscosity. The increased transport at 50˚W between experiments 14a and 14c corresponds to a depth independent increase in the downstream velocity at the jet axis of approximately 5 cm s^{-1} . On the other hand, the baroclinic component of the transport is nearly unchanged, implying that the vertical shear of the Gulf Stream above 1000 m is not as strongly sensitive to dissipation across this range of parameter space. The downstream transport in experiment 14c exceeds 180 Sv, substantially higher than any of the measured values (Hogg, 1992), though at a longitude that is not sampled by the observations. Within the limitations of the sparse observations, experiment 14b provides the closest agreement with the measured values.

The depth to which the variability of the Gulf Stream reaches increases with decreasing viscosity just as does the mean velocity. The eddy kinetic energy along 50˚W for experiments 13d2, 14a and 14c is shown in Figure 6. The near bottom eddy kinetic energy is nearly one order of magnitude smaller in experiment 13d2 than in experiment 14c. The weakness of both the deep mean flow and its variability lead us to anticipate that the interaction of the Gulf Stream with topography at the tail of the Grand Banks could be quite different for these experiments.

The variability of the path of the Gulf Stream has a distinctly different character as viscosity is reduced. Instantaneous paths of the Gulf Stream (defined by the 12˚C isotherm at 400m) at 10 day intervals over the period 1998 to 2000 for experiments 14a and 14c appear in Figure 7. The most dramatic differences are at the separation point. As noted above from the streamfunction, the separation point migrates south with decreasing viscosity; in experiment 14c to a latitude well outside the observed meander envelope. In addition, the breadth of the meander envelope becomes unrealistically large near the separation point. The path of the Gulf Stream following separation becomes increasingly zonal at lower viscosity. Further downstream, the meander envelope appears to tighten somewhat near 50˚ at the lowest viscosity. Experiment 14a provides the closest agreement with the observations of the mean position, curvature and envelope of the Gulf Stream west of 65˚W of these 0.1˚ experiments.

The spin-up of the circulation toward the states illustrated in Figures 2-5 takes place at differing paces depending on the viscosity. The streamfunction for cases 14a and 14c is shown in Figure 8 for the period 1990-1992 (years 5-7 of the experiment). The higher viscosity case has a separation characterized by a boundary eddy and the northern recirculation is confined primarily to the east of the NESC. In the lowest viscosity case, the recirculation is fully developed, and the separation has not yet moved south of Cape Hatteras. The boundary eddy in case 14a persists until about 1997, at which time the NRG reaches the separation point and the flow becomes more zonally oriented. The differences in the rate at which the pattern of the flow are established contrast with the spin-up of the basin-averaged KE which show comparable rates of convergence toward the asymptotic values for cases 14a through 14c.

3.2 The North Atlantic Current

SMBH point out the significant improvement in the simulation of the path of the North Atlantic Current (NAC) at 0.1˚ over coarser resolution models and the remarkable agreement with the observed time mean flow pattern in terms of the number and position of meanders along the western boundary. The flow at 730m depth in the region extending from the Grand Banks to the "Northwest Corner" for cases 14a and 14c is shown in Figure 9. The observed mean velocity on the WOCE ACM-6 line at depths between 734m and 781m reported by Schott et al. (2004) are shown for comparison. We see that the meander pattern and positions are quite consistent across this range of dissipation. After crossing the Southeast Newfoundland Rise the Current turns northwestward, forming the shoreward flank of the Mann Eddy, an anticyclonic feature centered near 42˚N and 43˚W, which emerges from a time-averaged view and is said to contain the warmest waters to be found at 1000m depth in the entire NA (Rossby 1996). Immediately to the north a cyclonic recirculation is found, followed by an anticyclonic meander near 45.5˚N. Closed eddies in the Northwest Corner, north of Flemish Cap, are also seen in each experiment. There is an eastward shift of the western edge of the Mann Eddy at the higher viscosity, such that the core of the NAC is displaced significantly off of the observed velocity maximum. As viscosity increases, the meanders also become more zonally elongated. This basic meander pattern persists even in the 0.2˚ experiments. However, while the meander pattern has strong similarities across these cases, the throughflow of the NAC changes substantially. With higher viscosity less fluid is recirculated to the north and west through each of the cyclonic meanders. More fluid is lost from the Grand Banks region to the east at lower latitudes, with less reaching the Northwest Corner. This can be seen more directly in Figure 10 showing the vertically integrated transport across 37˚W in each case. The eastward flow is concentrated into cores at 46˚N, 48˚N, 49.5˚N, and 51˚N (with broadening and merging at the lowest resolution). The strength of the interleaved westward flow increases at higher resolution and lower levels of dissipation. At higher viscosity, the meanders and eastward flow near 50˚N are supplied by water retroflecting from the Labrador Current east of Flemish Cap rather than subtropical waters flowing north in the NAC (Figure 9).

The changes in the throughflow of the NAC are seen to be associated with a dramatic shift in the thermal structure in the region. At the lowest viscosity, the front between subtropical and subpolar waters is tighter and oriented southwest-northeast, whereas at higher viscosity the front is more diffuse and zonal. In consequence, subtropical waters reach higher latitudes within and on the offshore side of the NAC and subpolar waters reach lower latitude along the western boundary at the lowest viscosity. The eastward spreading of subpolar waters in the higher viscosity and lower resolution experiments results in a very large sea surface temperature error relative to observations.

The transport of the time-averaged NAC across the WOCE ACM-6 section, as a function of density class is compared with the observations reported in Schott et al. (2004) in Table 2. This section captures the poleward transport of the NAC as it flows north around the Grand Banks. The total NAC transport is too weak by a factor of at least two, even in the least viscous case 14c. The weakness in NAC transport is particularly evident

in the upper ocean and within the bounds Schott et al. apply to Labrador Sea Water, which in this case would be comprised largely of waters recirculating in the Mann Eddy.

The simulated sea surface height variability can be compared with satellite observations, as was done in Le Traon et al. (2001) and Brachet et al. (2004) using case 13 of SMBH. The less viscous cases, 14b and 14c, not only have a more realistic southwest-northeast front, as discussed above, but also have rms amplitude of sea surface height variability in better agreement with observations, as shown in SMBH and Le Traon et al. (2001). Simulated sea surface height variability in the more viscous cases 14a, 13d2, and in the lower resolution cases is weak, indicating little penetration into the Northwest Corner. Although we do not show sea surface height variability, in the interest of brevity, we point out that while case 14a develops a very realistic Gulf Stream separation, and has signatures of the observed stationary recirculations in the Grand Banks and Northwest Corner regions, the poor simulation of the observed baroclinic structure of the NAC and NAC throughflow result in an underestimate of the variability of the flow. We also see a suppression of the Azores Current and its associated sea surface height variability with higher dissipation or lower horizontal resolution, whereas this feature was well reproduced in case 13 of SMBH and in the less viscous 14b and 14c cases here.

3.3 The Deep Western Boundary Current

A growing collection of observational estimates of the transport of the Deep Western Boundary Current (DWBC) based on direct velocity measurements [Dickson and Brown, 1994; Fischer et al, 2004; Schott et al. 2004; Pickart and Smethie, 1998; Joyce et al, 2005] provide a quantitative reference against which to compare our simulations. In Figure 11 we show the transport across a set of western boundary sections starting just south of Denmark Strait and extending to the western side of the NRG. In each case the transport is calculated from the time mean velocity field over the area below the time mean σ_θ=27.80 isopycnal and between the continental slope and the 0 cm s^{-1} isotach. This density surface is used in each of the cited studies to encompass water masses in the DWBC derived from Denmark Strait and the Iceland-Scotland Overflows.

With the exception of the 0.4˚ experiment, all of the experiments come within 1 Sv of the reported transport at Dohrn Bank, with a weak increase in transport for decreasing viscosity. The transport increases through entrainment and recirculation moving downstream to the Angmassalik and Cape Farewell sections. Again, with the exception of the 0.4˚ experiment, the increase exceeds that observed, and is larger in the lower viscosity cases. In contrast to observations, the 0.2˚ and 0.1˚ experiments show a further substantial increase in transport within this density range as the boundary current rounds the Labrador basin. While we have employed the same density range in computing transports as used in the observational studies, errors in the simulation of the water mass properties as well as the velocity fields contribute to the differences in transport seen in Figure 11. The excessive transport in the Labrador Sea section is primarily due to an over abundance of water in the density range σ_θ=27.80 to 27.88. Even in the least viscous experiment there is no indication of a bottom trapped velocity maximum seen in the observations [Fischer et al, 2004].

The observed transport of the DWBC decreases as it passes inshore of the NAC near 43˚N. As might be anticipated from the discussion above on the model simulated NAC, only the 0.1˚ experiments approach the observed transport of the DWBC here as it passes to the east of Newfoundland. In contrast to the situation upstream, only case 14c exceeds the observational estimate. The agreement with observations deteriorates as the DWBC rounds the tail of the Grand Banks and enters the NRG. All experiments substantially underestimate the westward transport on the section near 55˚W. Further, the trend of larger transports with lower dissipation seen upstream is reversed at this and the subsequent section. The agreement with observations improves somewhat at the final section near 70˚W, though with the counterintuitive result of the most viscous 0.1˚ experiment showing the highest transport.

There are systematic changes in the water mass properties in the Deep Western Boundary Current region across this range of experiments. This can be seen in Figure 12 illustrating the maximum density of water found on the bottom in the region downstream from Denmark Strait for the 0.1˚ experiments. With decreasing dissipation, higher density is maintained in the core of the DWBC.

4. Discussion

The southward displacement of the separation point of the Gulf Stream in the 0.1˚ experiments as viscosity decreases is suggestive of the behavior first seen in the simulations of Thompson and Schmitz (1989) where the Stream was displaced to the south as the strength of the imposed Deep Western Boundary Current increased. Dietrich et al. (2004) invoke the same mechanism to rationalize the change in separation behavior of the Gulf Stream in their model as viscosity is decreased. That is, they attribute the change in the upper ocean circulation not to a local direct response to the change in dissipation, but rather to an indirect response to changes occurring in the deep circulation that are in turn determined by dissipation changes. The strengthening of the deep outflow from the Labrador Sea seen in Figure 11 and the increase in the strength of the NRG in our experiments are consistent with this view. However, the changes in the component of the DWBC transport derived from overflow waters do not make a strong contribution to the total barotropic transport differences. There is an additional increase in the transport of waters identified with Labrador Sea Water (density range σ_θ=27.68 to 27.80), which being higher in the water column, could have a more direct dynamical impact on the dynamics of the Gulf Stream. Further, the concomitant increase in the transport of the southern recirculation gyre suggests that eddy driving of the NRG may also be an important component of the changes seen with decreasing viscosity and increasing resolution.

Another view of the dependence of the separation on viscosity is provided by Özgökmen et al. (1997). They attribute the transition from "boundary eddy" to jet separation and the development of the southern recirculation gyre to a transition from a viscously dominated to inertially dominated flow regime. Our results are consistent with this picture as well, up to a point. The departure from the Özgökmen et al. (1997) study concerns the variability of the Stream at the separation point. They suggest that in order to separate as a jet, a stable upper ocean flow with weak eddy kinetic energy on the boundary is required, such that the flow remains primarily baroclinic and isolated from the influence of topography. The increase in variability on the boundary while the separation point moves south with decreasing viscosity in the present cases (Figure 7) runs counter to this conjecture.

The North Atlantic Current and Gulf Stream separation are obviously interdependent. The GS is the source of what becomes the NAC, though the Current is influenced by topography (New England Seamount Chain, Grand Banks), by the strong recirculations which join its flanks, and by surface forcings (at least at shallower depths; note that a water parcel might typically take something like 2 to 6 months to get from Hatteras to the Grand Banks). The northern recirculation gyre, which in turn is fed by inflow from the Labrador Sea, is more vigorous in cases in which the Stream separates, though as discussed above causality remains unclear. We note that we have not seen the NAC turn the corner around the Grand Banks and Flemish Cap without good Gulf Stream

separation. In contrast, we have seen good Gulf Stream separation without a good simulation of the Northwest Corner (e.g. experiment 14a).

Though we don't find support for the Özgökmen et al (1997)deep eddy energy hypothesis at Cape Hatteras, we do find that higher eddy kinetic energies near the bottom, below the Gulf Stream, and a greater degree of vertical penetration are associated with a better simulation of the NAC. This is consistent a stronger topographic influence on the course of the NAC as it crosses the tail of the Grand Banks and the Newfoundland seamounts.

The absence of the boundary eddy in the early phases of the experiment described in SMBH can be attributed, in part, to the viscosity bug. The extra factor of dx^3 in the scaling resulted in the viscosity at 35˚N being about 50% of the intended value, or comparable to that used in experiment 14b. Further, the initial stages of that experiment used an equatorial value of viscosity that was 1/3 the now standard value. In short, experiment 13d was spun-up with lower dissipation than experiment 14a, with the result being an earlier development of the recirculation gyres and a better representation of the NAC.

5. Conclusions

The southward displacement of the Gulf Stream separation and subsequent overly zonal path at the lowest value of viscosity (case 14c), demonstrates that horizontal dissipation cannot be reduced to the stability limit, even at what we would call an eddy-resolving 0.1˚ resolution. Eddy viscosity is still required to provide closure, emphasizing our confirmation (not unexpected) that our simulations are not yet in a convergent regime, except perhaps in the case of convergence to a poor and unrealistic solution at undesirably high values of dissipation. High-resolution ocean model simulations, though less sensitive to the details of subgrid-scale closure than eddy-permitting and non-eddy-resolving models, retain an appreciable sensitivity to the closure scheme. We expect these points to apply to simulations with forms of isopycnal tracer mixing and anisotropic viscosity as well.

In our regional North Atlantic simulations we found it possible to achieve good Gulf Stream separation, a realistic Azores Current and North Atlantic Current penetration into the Northwest Corner region with intermediate values of biharmonic horizontal viscosity and diffusivity (our 14b case). With too little dissipation we get, as mentioned just above, an overly zonal and southward displaced Gulf Stream separation. The more dissipative extreme in this tuning exercise suppresses the downstream features leading to very large SST errors at the subtropical-subpolar gyre boundary. In our experience, a relatively small region in parameter space exists in which these features are well balanced.

The success of the circulation published in SMBH is therefore partially a result of good fortune in the choice of dissipation coefficients. That success should probably also be taken as support for the preservation of grid-Reynolds and grid-Peclet numbers with

variable resolution, as mentioned in the Model Configuration section, and which we have long used as a rule-of-thumb (the basis for this scaling can be found in the Appendix of Bryan et al. 1975, and in Chapter 18 of Griffies 2004) . The initial values of dissipation chosen in SMBH were based on such a scaling from the experience of Maltrud et al. (1998) at eddy-permitting resolution. The results also suggest that further exploration of subgrid-scale closure schemes for simulations in this resolution range is warranted. One such investigation has already been completed: Smith and Gent (2004) demonstrate improvement in some aspects of the North Atlantic circulation in POP with the use of an anisotropic form of isopycnal mixing and anisotropic viscosity (Smith and McWilliams 2003), even at 0.1° resolution.

Our investigation has been motivated by the need to understand how best to configure an eddy-resolving ocean model for high-resolution climate modeling, an effort soon to be realized. The regional North Atlantic context is attractive for such investigation, being roughly a factor of eight less expensive than a fully global ocean simulation. We must express a note of caution however, that our results may not generalize entirely to other similar model configurations, as our experience (with a larger group of collaborators) suggests that differences in the representation of topography and lateral boundary conditions (restoring at our northern and southern boundaries, open in a fully global model) may exert significant influence over the simulated North Atlantic Ocean circulation.

Acknowledgments

F. Bryan's work at the National Center for Atmospheric Research is sponsored by the National Science Foundation. M. Hecht, R. Smith and the computers on which these simulations were run were supported by the Climate Change Prediction Program in the U.S. Department of Energy's (DOE) Office of Science. LANL is operated by the University of California for DOE under contract W-7405-ENG-36.

References

Barnier, B., L. Siefridt, and P. Marchesiello, 1995. Thermal forcing for a global ocean circulation model using a three–year climatology of ECMWF analyses. *J. Mar. Syst*., **6**, 363–380.

Beckmann, A., C.W. Böning, C. Köberle, and J. Willebrand, 1994. Effects of increased horizontal resolution in a simulation of the North Atlantic Ocean. *J. Phys. Ocean*., **24**, 326–344.

Bracco, A., E.P. Chassignet, Z.D. Garraffo, and A. Provenzale, 2002. Lagrangian velocity distributions in a high-resolution numerical simulation of the North Atlantic. *J. Atmos. Ocean. Tech*., **20**, 1212–1220.

Brachet, S., P.Y. LeTraon, and C. LeProvost, 2004. Mesoscale variability from a high-resolution model and from altimeter data in the North Atlantic Ocean. *J. Geophys. Res*., **109**, doi:10.1029/2004JC002360.

Bryan, F.O., C.W. Böning and W.R. Holland, 1995. On the mid-latitude circulation in a high resolution model of the North Atlantic. *J. Phys. Ocean.,* **25**, 289–305, 1995.

Bryan, K., S. Manabe and R. C. Pacanowski, 1975. A global ocean-atmosphere climate model. Part II. The oceanic circulation. *J. Phys. Ocean.,* **5**, 30–46.

Cessi, P. 1991. Laminar separation of colliding western boundary currents. *J. Mar. Res*., **49**, 697–717.

Chao, Y.-C., A. Gangopadhyay, F.O. Bryan and W.R. Holland, 1996. Modeling the Gulf Stream: How far from reality? *Geophys. Res. Lett.,* **23**, 3155–3158.

Dengg, J., A. Beckmann, and R. Gerdes, 1996: The Gulf Stream separation problem. *The Warmwatersphere of the North Atlantic Ocean*, W. Krauss, Ed. Gebruder-Borntrager, 253–290.

Dickson, R.R. and J. Brown, 1994. The production of North Atlantic Deep water: Sources, rates and pathways. *J. Geophys. Res.,* **99**, 12319–12341.

Dietrich, D.E., A. Mehra, R.L. Haney, M.J. Bowman and Y.H. Yang, 2004. Dissipation effects in North Atlantic ocean modeling. *Geophys. Res. Lett.*, **31**, L050302, doi:10.129/2003GL019015.

Dukowicz, J.K. and R.D. Smith, 1994. Implicit free-surface method for the Bryan-Cox-Semtner ocean model. *J. Geophys. Res*., **99**, 7991–8014.

Fischer, J., F.A. Schott, M. Dengler, 2004. Boundary circualation at the exit of the Labrador Sea. *J. Phys. Ocean*., **34**, 1548–1570.

Gent, P.R. and J.C. McWilliams, 1990. Isopycnal mixing in ocean circulation models. *J. Phys. Ocean.*, **20**, 150–155.

Griffies, S.M., 2004. *Fundamentals of Ocean Climate Models.* Princeton University Press, 518 pp.

Hogg, N., 1992. On the transport of the Gulf Stream between Cape Hatteras and the Grand Banks. *Deep-Sea Res*., **39A**, 1231–1246.

Hurlburt, H.E. and P.J. Hogan, 2000. Impact of 1/8˚ to 1/64˚ resolution on Gulf Stream model-data comparisons in basin-scale subtropical Atlantic models. *Dyn. Atmos. Ocean.,* **32**, 283–329.

Johns, W.E., T.J. Shay, J.M. Bane, and D.R. Watts, 1995. Gulf Stream structure, transport, and recirculation near 68˚W. *J. Geophys. Res.,* **100**, 817-838.

Joyce, T.M., J. Dunworth-Baker, R.S. Pickart, D. Torres and S. Waterman, 2005. On the Deep Western Boundary Current south of Cape Cod. *Deep-Sea Res. II*, **52**, 615–625.

Le Traon, P.Y. and G. Dibaroure and N. Ducet, 2001. Use of a high-resolution model to analyze the mapping capabilities of multiple-altimeter missions *J. Atmos. Ocean. Tech*., **18**, 1277–1288.

Levitus, S., 1982. *Climatological Atlas of the World Ocean*. NOAA Prof. Paper No 13, U.S. Govt. Printing Office, Washington, D.C., 173 pp.

Maltrud, M.E., R. D. Smith, A. J. Semtner and R. C. Malone, 1998; Global eddy-resolving ocean simulations driven by 1985-1994 atmospheric winds. *J. Geophys. Res*., **103**, 30825–30853.

McClean, J.L., P.-M. Poulain, J.W. Pelton and M.E. Maltrud, 2002. Eulerian and Lagrangian statistics from surface drifters and a high resolution POP simulation in the North Atlantic. *J. Phys. Ocean*., **32**, 2472–2491.

Oschlies, A., 2002. Improved representation of upper-ocean dynamics and mixed-layer depths in a model of the North Atlantic on switching from eddy-permitting to eddy resolving grid resolution. *J. Phys. Ocean.,* **32**, 2277–2298.

Özgökmen, T.M., E.P. Chassignet, and A.M. Paiva, 1997. Impact of wind forcing, bottom topography, and intertia on midlatitude jet separation in a quasigeostrophic model. *J. Phys. Ocean.*, **27**, 2460–2476.

Paiva, A.M., J.T. Hargrave, E.P. Chassignet, and R. Bleck, 1998. Turbulent behavior of a fine-mesh (1/12˚) numerical simulation of the North Atlantic. *J. Mar. Sys.,* **21**, 307–320.

Pickart, R.S. and W.M. Smethie Jr., 1998. Temporal evolution of the Deep Western Boundary Current where it enters the sub-tropical domain. *Deep-Sea Res. I*, **45**, 1053–1083.

Rossby, T., 1996. The North Atlantic Current and surrounding waters: At the crossroads. *Rev. Geophys*, **34**, 463–481.

Schott, F.A., R. Zantopp, L. Stramma, M. Dengler, J. Fischer and M. Wibauz, 2004. Circulation and deep-water export at the western exit of the subpolar North Atlantic. *J. Phys. Ocean*., **34**, 817–843.

Smith, R.D. and P.R. Gent, 2004. Anisotropic GM parameterization for ocean models. *J. Phys. Ocean*., **34**, 2541–2564.

Smith, R.D. and J.C. McWilliams, 2003. Anisotropic horizontal viscosity for ocean models. *Ocean Modelling,* **5**, 129–156.

Smith, R.D., M.E. Maltrud, F.O. Bryan and M.W. Hecht, 2000. Numerical simulation of the North Atlantic Ocean at 1/10˚. *J. Phys. Ocean*., **30**, 1532–1561.

Thompson, J.D. and W.J. Schmitz, 1989. A limited-area model of the Gulf Stream: Design, initial experiments and model-data intercomparison. *J. Phys. Ocean*., **19**, 791–814.

Watts, D.R., K.L. Tracey, J.M. bane, and T.J. Shay, 1995. Gulf Stream path and thermocline structure near 74˚W and 68˚W. *J. Geophys. Res.,* **100**, 18,291–18312.

Willebrand, J., B. Barnier, C. Böning, C. Dieterich, P.D. Killworth, C. Le Provost, Y. Jia, J.-M. Molines, and A.L. New, 2001. Circulation characteristics in three eddy-permitting models of the North Atlantic. *Prog. Ocean.,* **48**, 123–161.

Name	Resolution	C	L_{Munk} (km)	Initial Condition	Run Length (years)
14a	0.1˚	1	15.7	Resting @ 1/1/1986	15
14b	0.1˚	0.5	13.7	Resting @ 1/1/1986	15
14c	0.1˚	0.25	11.9	Resting @ 1/1/1986	15
13d	0.1˚	1	15.7	Exp 13 @ 1/1/1987	5
13d2	0.1˚	8	23.9	Exp 13 @ 1/1/1987	5
15d	0.2˚	1	23.9	Exp 15 @ 1/1/1987	5
15f	0.2˚	0.125	15.7	Exp 15d @ 1/1/1992	5
17d	0.4˚	1	36.2	Resting @ 1/1/1985	20

Table 1. Summary of Experiments.

Experiment	Period	Upper	ULSW	LSW	GFZW	DSOW	Total
17d	1989-1991	18.1	0.2	0.3	1.0	1.5	21.1
15d	1989-1991	18.0	1.2	3.2	5.3	2.3	29.9
15f	1989-1991	24.3	1.9	7.1	9.9	4.3	47.4
13d2	1989-1991	18.1	0.9	2.6	2.4	1.5	25.6
13d	1989-1991	35.3	1.7	5.7	5.3	4.4	52.4
14a	1998-2000	23.8	1.7	8.5	7.5	5.3	46.9
14b	1998-2000	34.6	2.6	10.6	11.7	7.7	67.3
14c	1998-2000	37.3	2.4	10.5	12.5	8.4	71.0
Observed	1993-1995	81.2	9.2	23.4	16.4	11.4	142

Table 2. Density class mass transports, from a nearly zonal section between 42 and 43˚N. Model-diagnosed transports extend 500km out from the coast of the Grand Banks. The observations included below are from Schott et al. (2004). We use their definitions of water masses as a function of $\sigma_\theta$as well: Upper Labrador Sea Water, 27.68-27.74; Labrador Sea Water, 27.74-27.80; Gibbs Fracture Zone Water, 27.80-27.88; and Denmark Strait Overflow Water, σ_θ>27.88.

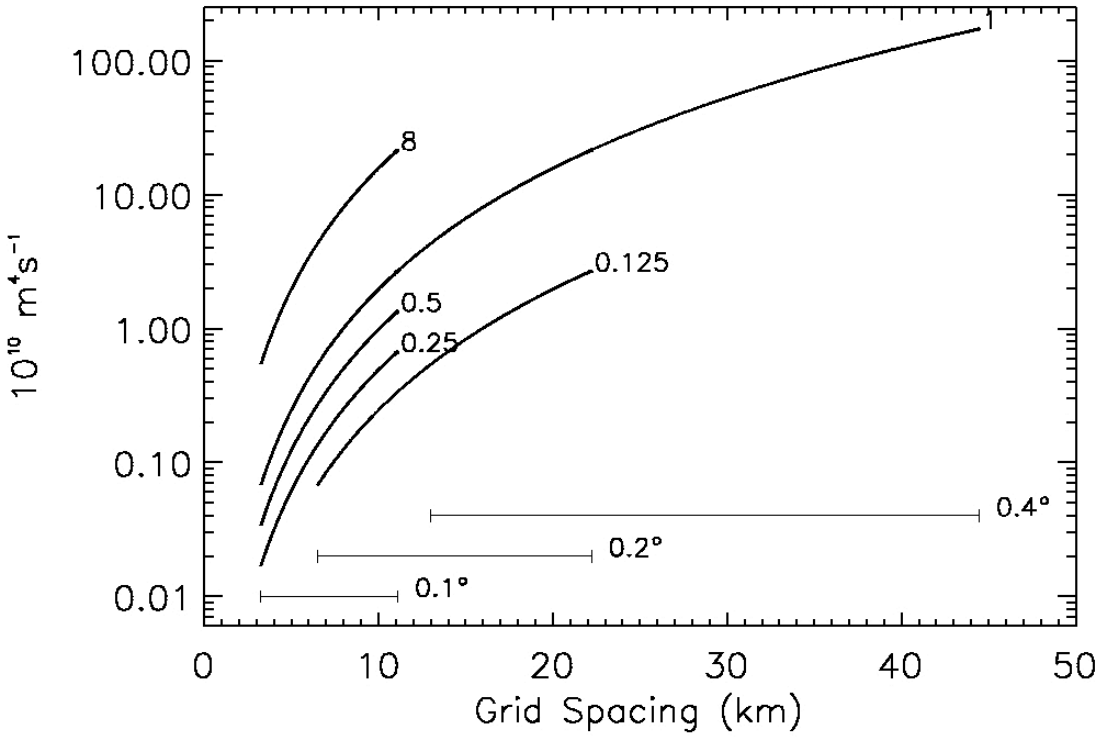

Figure 1. Magnitude of the horizontal hyperviscosity for each experiment as a function of horizontal grid size. Parameter C from Equation 2 is indicated next to each curve. The range of grid spacing on each of the three grids is indicated by the horizontal bars at the bottom.

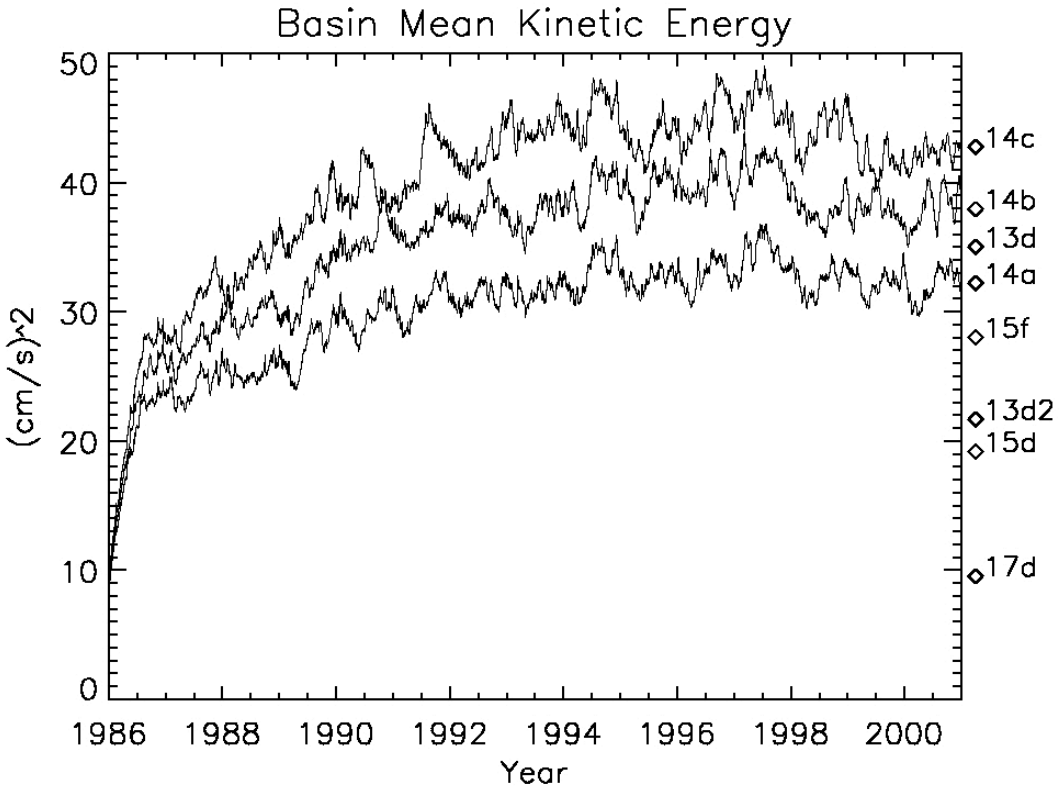

Figure 2. Timeseries of global mean kinetic energy for experiments 14a (lower), 14b (middle) and 14c (upper). The mean kinetic energy for the last three years of each experiment is indicated along the right hand margin.

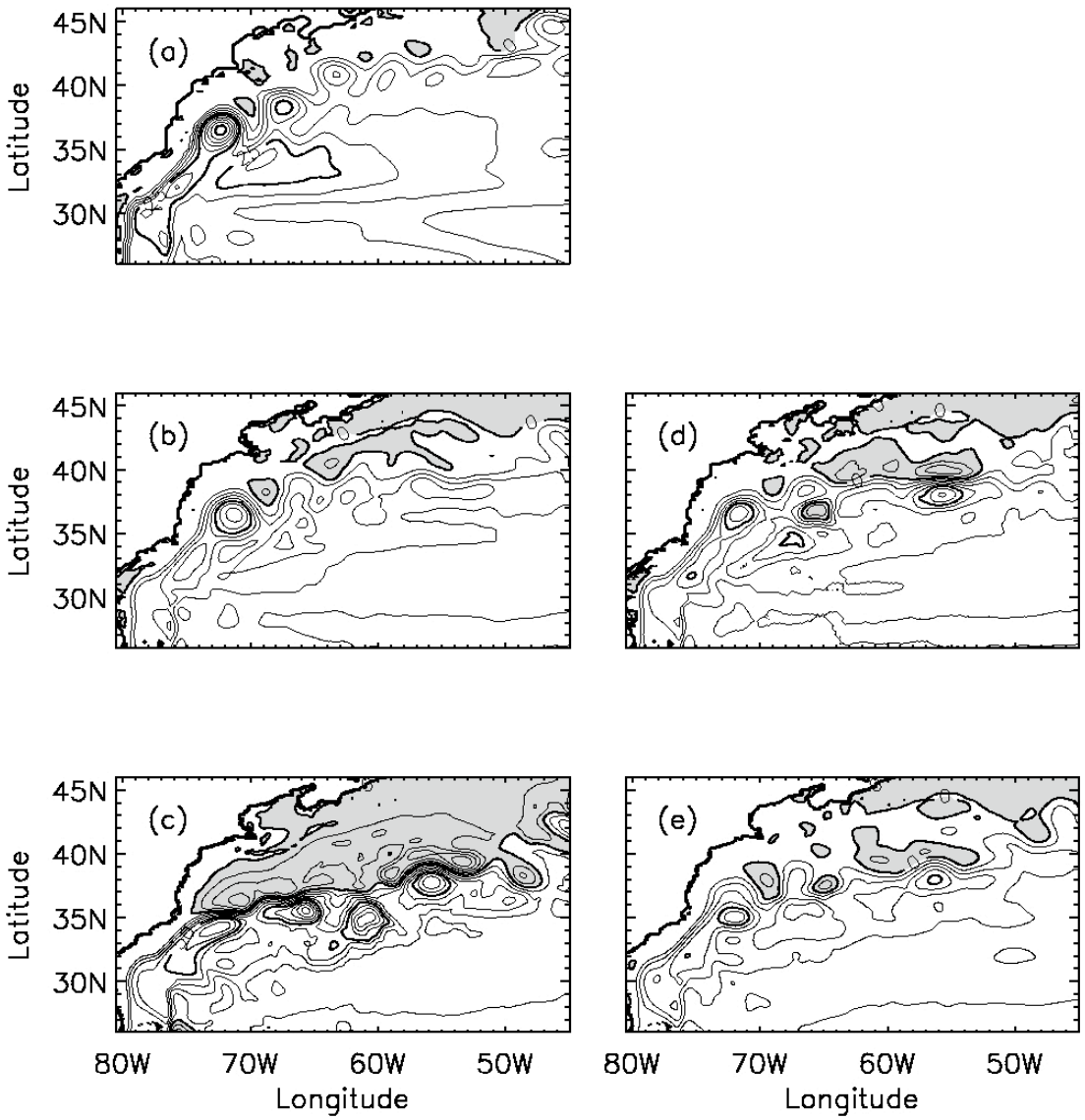

Figure 3 Streamfunction for the vertically integrated mass transport for experiments: a.) 17d b.) 15d c.) 13d d.) 15f e.) 13d2. Contour interval interval=10 Sv (5 Sv in panel a only).

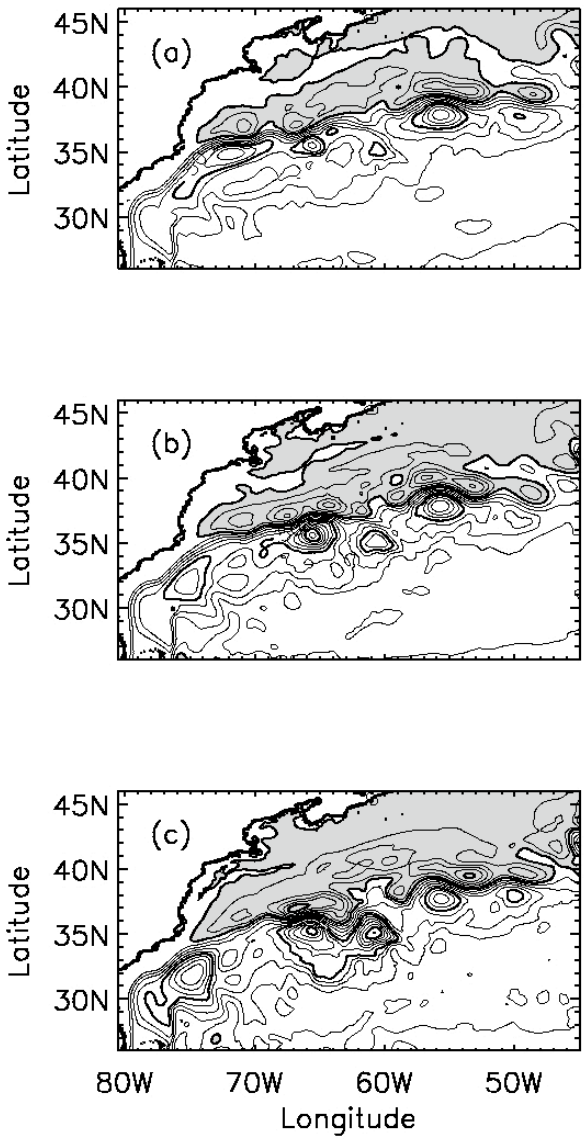

Figure 4. Streamfunction for the vertically integrated mass transport for experiments a.) 14a b.) 14b c.) 14c. Contour interval = 10 Sv.

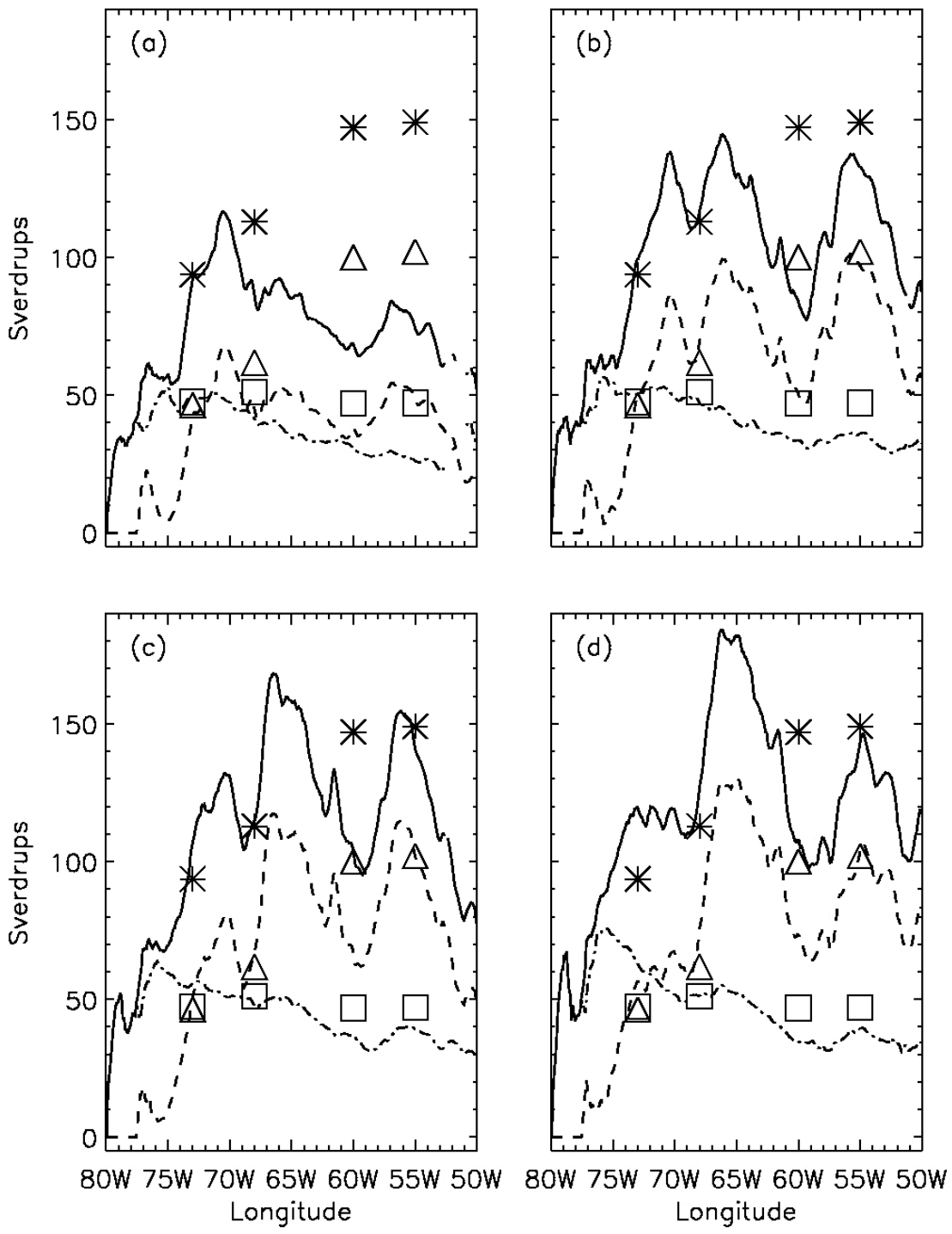

Figure 5. Downstream transport of the Gulf Stream computed in stream coordinates for experiments: a.) 13d2 b.) 14a c.) 14b d.) 14c. Lines represent simulation results, symbols observations from Hogg (1992) and Johns et al (1995). Solid curve and stars are total transport, dashed curve and triangle are barotropic transport and dash-dot curve and squares are baroclinic transport. Decomposition into barotropic and baroclinic follows the definitions of Hogg (1992).

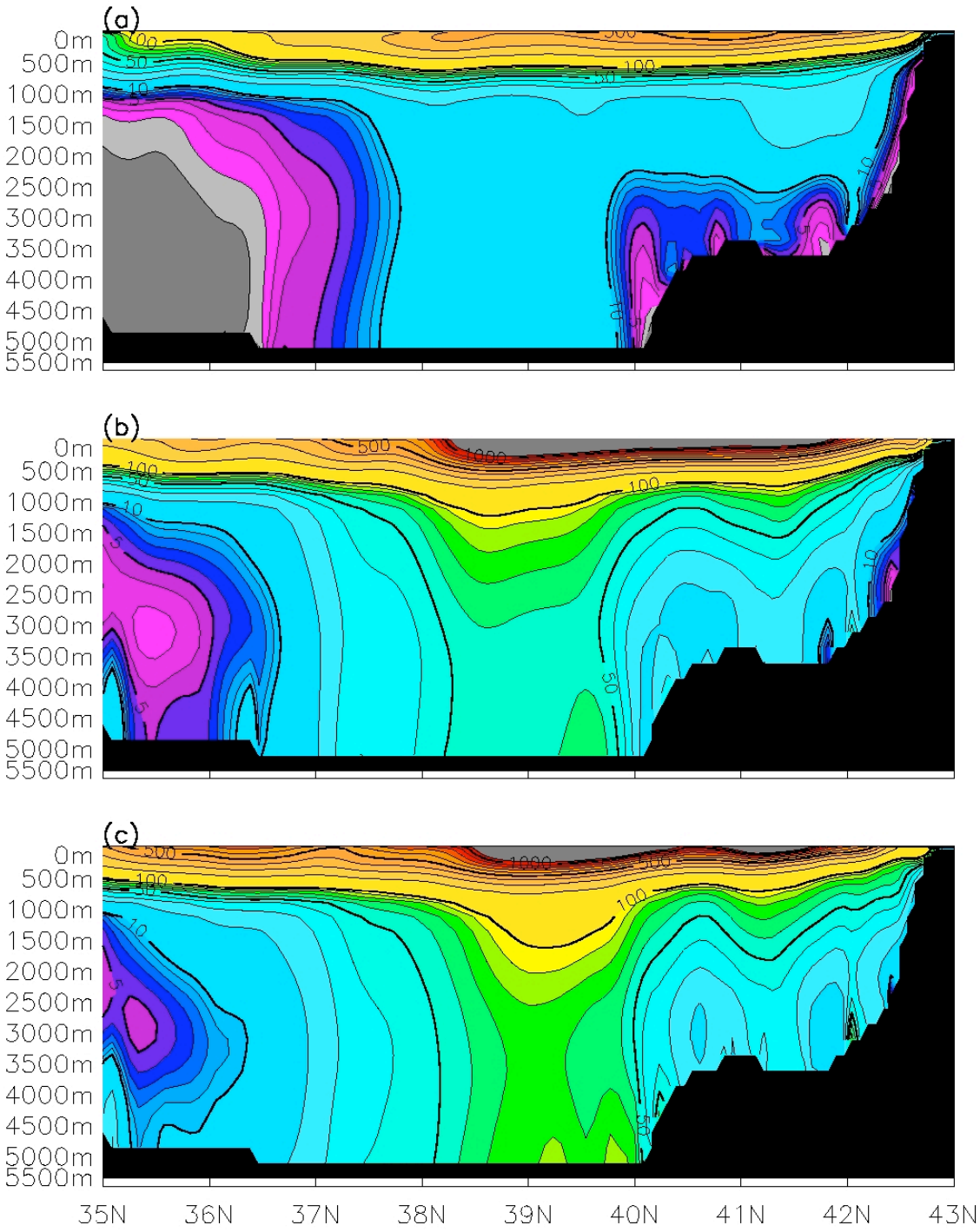

Figure 6. Eddy kinetic energy at 50°W for experiments a.) 13d2 b.) 14a c.) 14c. Logarithmic contour scale with contours at multiples of 1,2,3,… cm^2s^{-2}.

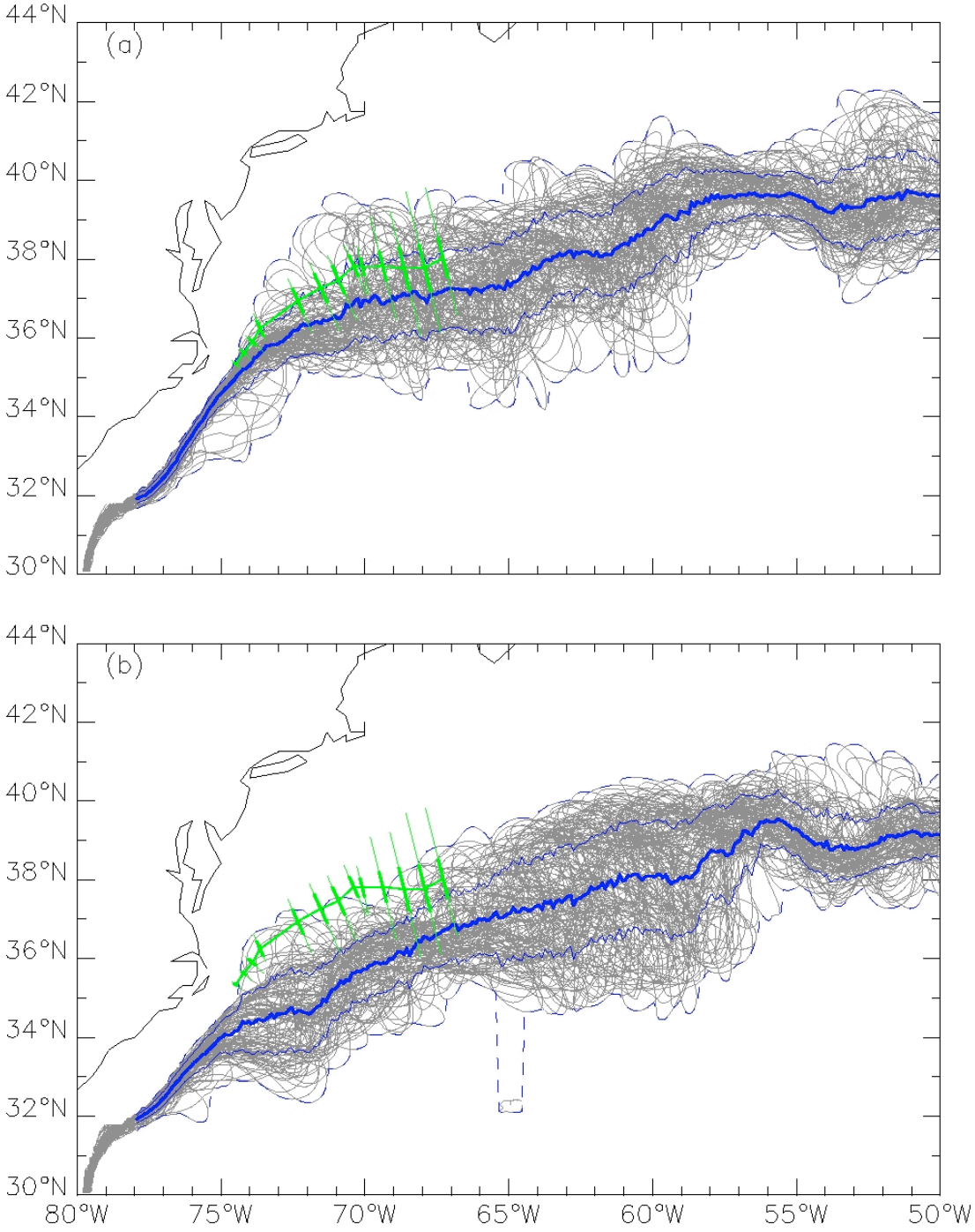

Figure 7. Gulf Stream position defined by the 12˚C isotherm at 400m every 10 days during 1998-2000 for experiments: a.) 14a b.) 14c. The time mean position and one standard deviation envelope are indicated by solid blue curves. Observed position and variability from Watts et al (1995) indicated in green.

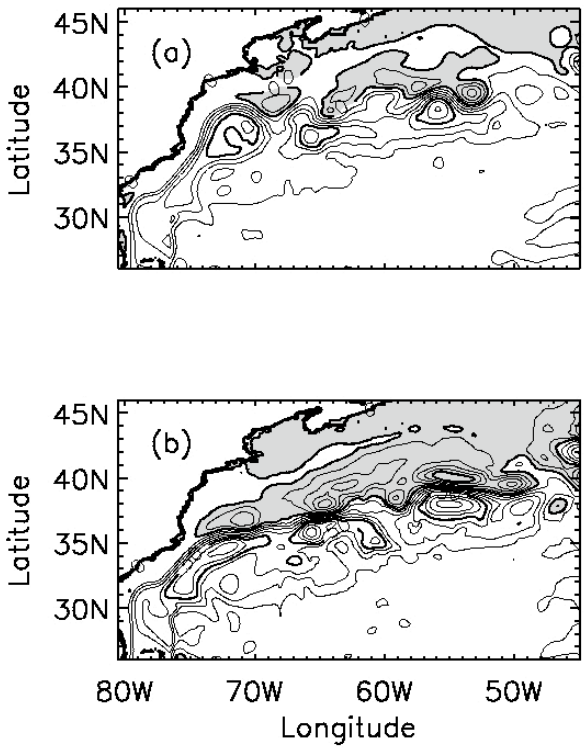

Figure 8. Streamfunction for the vertically integrated mass transport for 1990-1992 for experiments: a.) 14a b.) 14c. Contour interval = 10 Sv.

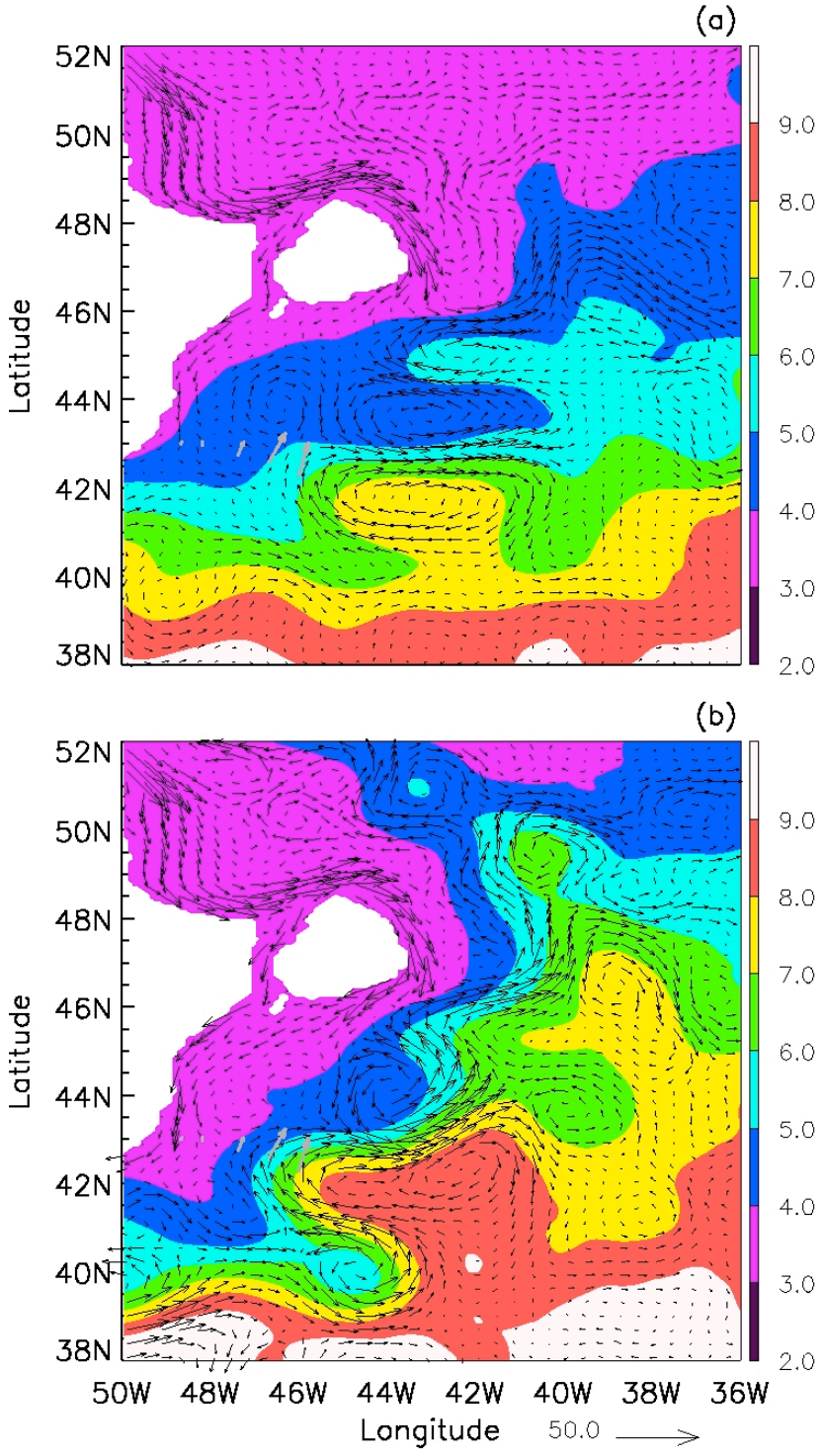

Figure 9. Velocity and potential temperature at 730m during 1998-2000, for experiments: a.) 14a, and b.) 14c. Grey arrows show observed mean velocity near this depth level as reported by Schott et al. (2004).

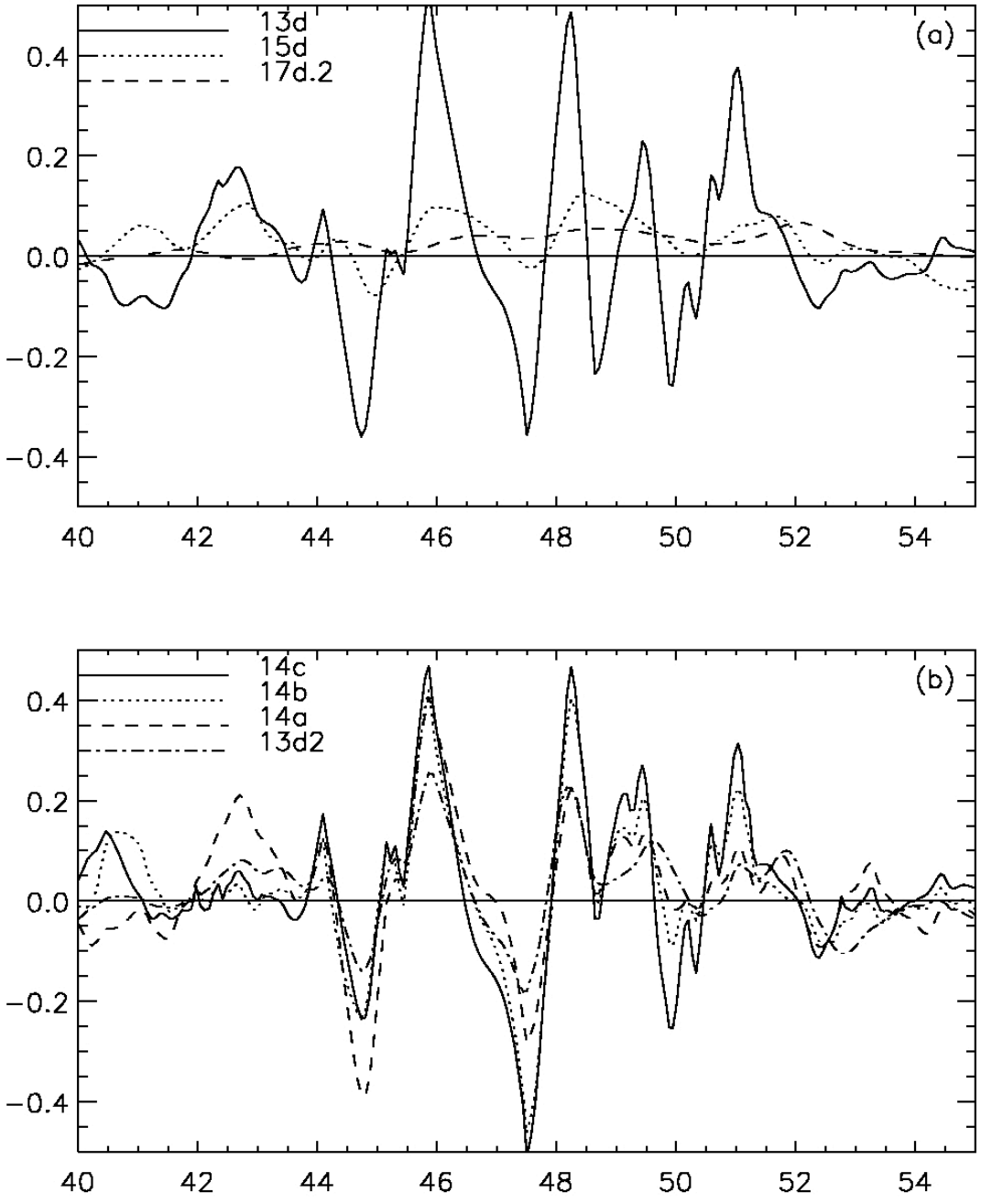

Figure 10. Vertically integrated transport (Sverdrups/km) across 37˚W a.) 0.4˚, 0.2˚, and 0.1˚ experiments with viscosity on the C=1 curve. b.) 0.1˚ cases with differing viscosity.

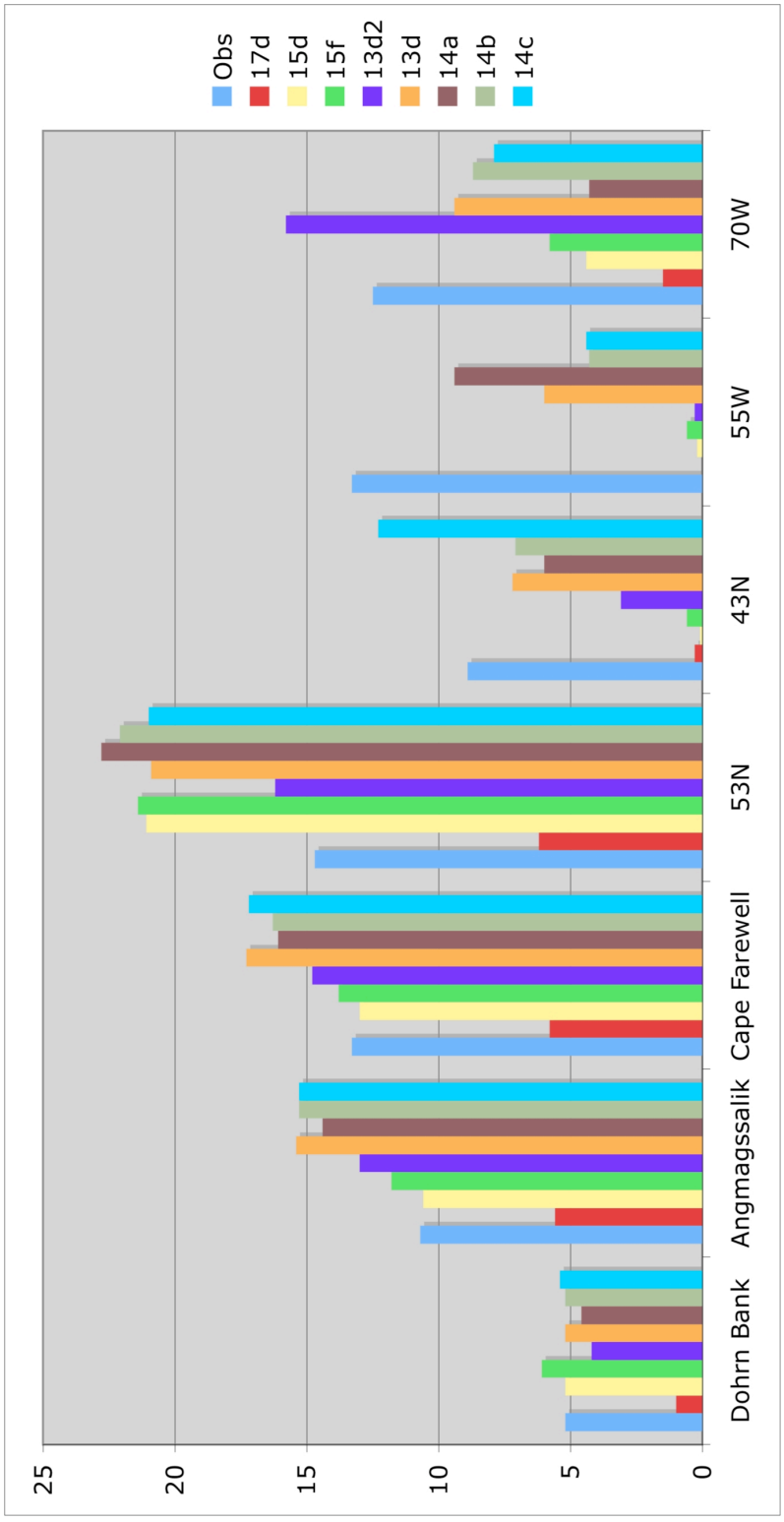

Figure 11. Transport (Sverdrups) of the Deep Western Boundary Current for density greater than σ_θ=27.80 across sections with observational estimates. Dohrn Bank, Angmassalik and Cape Farewell from Dickson and Brown [1994]. 53˚N from Fischer et al. [2004]; 43˚ from Schott et al. [2004]; 55˚W from Pickart and Smethie [1998]; 70˚W from Joyce et al. [2005].

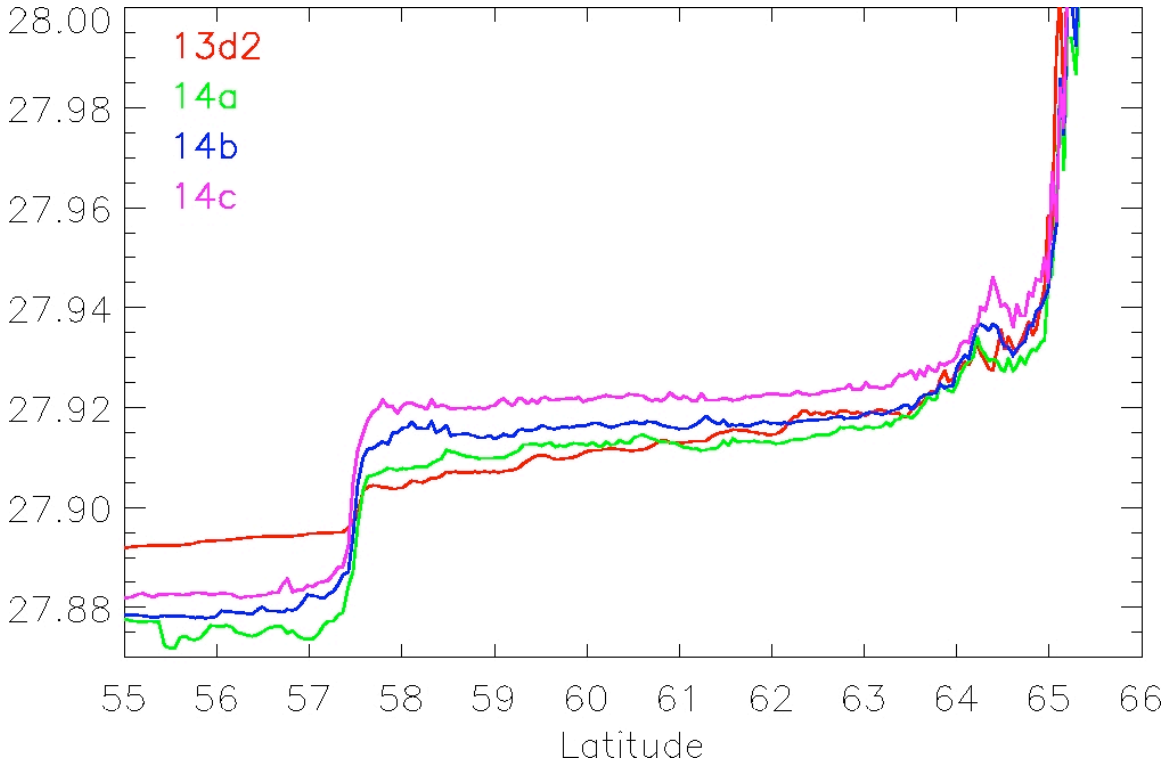

Figure 12. Maximum potential density within the longitude range 25˚W to 45˚ for the 0.1˚ experiments.